ACS Photonics

Letter

pubs.acs.org/journal/apchd5

Optical Transitions in Direct-Bandgap $Ge_{1-x}Sn_x$ Alloys

D. Stange,[†,⊥] S. Wirths,[†,⊥] N. von den Driesch,[†] G. Mussler,[†] T. Stoica,[†,‡] Z. Ikonic,[§] J. M. Hartmann,[∥] S. Mantl,[†] D. Grützmacher,[*,†] and D. Buca[*,†]

[†]Peter Grünberg Institute 9 (PGI 9) and JARA-Fundamentals of Future Information Technologies, Forschungszentrum Juelich, 52425 Juelich, Germany

[‡]National Institute of Materials Physics, P.O. Box MG-7, Magurele, Bucharest 077125, Romania

[§]Institute of Microwaves and Photonics, School of Electronic and Electrical Engineering, University of Leeds, Leeds LS2 9JT, United Kingdom

[∥]University of Grenoble Alpes, F-38000 and CEA, LETI, MINATEC Campus, F-38054 Grenoble, France

ABSTRACT: A comprehensive study of optical transitions in direct-bandgap $Ge_{0.875}Sn_{0.125}$ group IV alloys via photoluminescence measurements as a function of temperature, compressive strain and excitation power is performed. The analysis of the integrated emission intensities reveals a strain-dependent indirect-to-direct bandgap transition, in good agreement with band structure calculations based on the 8-band $k{\cdot}p$ and deformation potential methods. We have observed and quantified Γ valley−heavy hole and Γ valley−light hole transitions at low pumping power and low temperatures in order to verify the splitting of the valence band due to strain. We will demonstrate that the intensity evolution of these transitions supports the conclusion about the fundamental direct bandgap in compressively strained GeSn alloys. The presented investigation, thus, demonstrates that direct-bandgap group IV alloys can be directly grown on Ge-buffered Si(001) substrates despite their residual compressive strain.

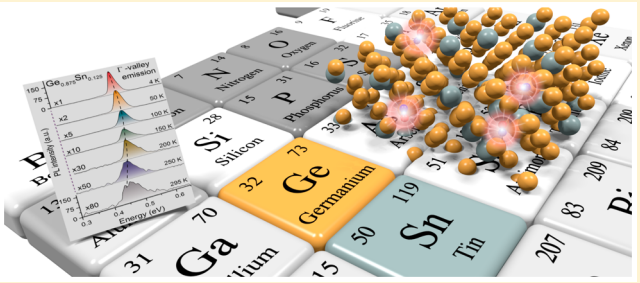

KEYWORDS: *direct bandgap, photoluminescence, germanium tin, group IV, compressive strain*

Group IV semiconductors are known for their excellent electronic transport properties but limited optical applicability due to their indirect-bandgap nature, turning them into inefficient light emitters. However, the pioneering work of R. Soref and C. H. Perry[1] and, later, He and Atwater[2] as well as subsequent theoretical studies[3−5] indicated that alloying two group IV elements, i.e., semiconducting Ge and semimetallic α-Sn, should result in a group IV semiconductor that could be tuned from an indirect- to a fundamental direct-bandgap material by increasing the substitutional Sn concentration in the Ge lattice. Although it was unanimously accepted that the Γ-valley of the conduction band can be decreased below the L-valley, theoretical estimates of the required Sn content for this transition as well as the impact of strain on the transition are widely spread.[6,7] This prospect has driven large efforts to grow device-grade GeSn epilayers,[8−11] to prove their fundamental direct bandgap, and finally to demonstrate photonic functionality. Recently, advances in chemical vapor deposition (CVD) of GeSn binaries with high Sn contents of up to 14% have been reported[9,10,12−15] that enabled not only the proof of the direct-bandgap nature but also the unambiguous demonstration of laser action at 2.3 μm under optical pumping.[16] Hence, direct-bandgap GeSn alloys are CMOS-compatible IV−IV semiconductors with novel optical and electrical properties that are similar to those of III−V and II−VI compounds, used today in optoelectronic applications, i.e., light-emitting diodes (LED) or laser diodes. This progress along with the recent developments of high-speed optical detection[17] and low-loss optical fibers[18] may pave the way toward 2 μm communications based on silicon photonics.[19]

However, in contrast to their III−V counterparts, GeSn binaries are either just direct or exhibit only a rather small directness, $\Delta E_{L\text{-}\Gamma} \geq 0$, with $\Delta E_{L\text{-}\Gamma}$ being the energy difference between the L- and Γ-valleys. Understanding the basic physical properties, i.e., the radiative recombination mechanisms of excess carriers, of these group IV materials, exhibiting a direct bandgap, is essential for further exploitation of GeSn as an active gain material for lasers, the only missing monolithically integrated Si photonic device.[20] Regardless of the recent breakthrough in lasing and the observation that the transition from an indirect to a direct bandgap occurs at about 9% Sn for cubic GeSn alloys,[16] only scattered experiments on optical transitions in GeSn alloys have been reported. The studies were restricted to room temperature and/or low Sn contents, e.g., below the indirect to direct transition.[10,21−23] Therefore, we have performed detailed photoluminescence (PL) measurements on CVD-grown GeSn alloys at various temperatures and excitation powers. We show that for a constant Sn content of approximately 12.5% a variation of compressive strain induces

Received: July 7, 2015
Published: October 14, 2015

DOI: 10.1021/acsphotonics.5b00372
ACS Photonics 2015, 2, 1539−1545

the fundamental transformation from an indirect to a direct bandgap. Furthermore, the splitting of the direct PL transitions into distinct contributions stemming from heavy hole (HH) and light hole (LH) valence bands is studied experimentally and theoretically.

The GeSn films were grown on 200 mm Si wafers with 3 μm thick Ge buffers (Ge-VS, previously grown with a separate CVD system)[24] using reduced pressure chemical vapor deposition with Ge_2H_6 and $SnCl_4$ as precursor gases.[9,15] The growth temperature (350 °C), the total pressure, and the partial pressures of the source gases were kept constant, resulting in the growth of GeSn alloys with a Sn content of 12.5 ± 0.5 at. %.[11,15] Due to the lattice mismatch between the GeSn film and Ge virtual substrate, the GeSn layers were biaxially compressively strained. The films are fully strained for thicknesses below the critical thickness for strain relaxation (~50 nm), while they plastically relax via the formation of misfit dislocations for larger thicknesses. The residual strain depends sensitively on the thickness beyond the critical value.[11] Rutherford backscattering spectrometry (RBS) was used to determine the Sn content and the layer thickness, while the strain was measured by X-ray diffraction using reciprocal space mapping (XRD-RSM).[11] An overview of the investigated samples is given in Table 1.

Table 1. Overview of the Investigated GeSn Samples: Sn Content, Layer Thickness, Compressive Strain, Computed Directness $\Delta E_{L\text{-}\Gamma}$, and Experimental Deactivation Energy E_A of the Photoluminescence

sample no.	Sn content (±0.5 at. %)	thickness (±5 nm)	strain (±0.15%)	calculated $\Delta E_{L\text{-}\Gamma}$ (meV)	deactivation energy E_A (meV)
A	12	46	−1.65	−57	47[a]
B	13	172	−1.05	6	17.6
C	12.5	280	−0.48	44	22.5
D	12.5	414	−0.41	50	32.4
E	12.5	560	−0.4	50	26.5

[a]For indirect gap sample A, E_A is the activation energy of the PL at room temperature

RESULTS AND DISCUSSION

Electronic band structure calculations in the vicinity of the Γ-point for $Ge_{0.875}Sn_{0.125}$ with different compressive strain levels were performed using the 8-band $k\cdot p$ method[25] and the conventional deformation potentials for indirect valleys. The band structure of $Ge_{0.875}Sn_{0.125}$ at 295 K as a function of biaxial compressive strain is shown in Figure 1. GeSn alloys under large compressive strain are indirect semiconductors; according to our calculations, the transition to a direct bandgap is expected to occur at a strain of approximately −1.05%. The largest bandgap is found at the crossover of Γ- and L-bands, where the bandgap changes from indirect to direct. This reveals a remarkable property of GeSn grown on Ge-buffered Si(001): indirect and direct alloys with identical bandgap energies can be accessed simply by tuning the strain. The partially filled parabolas indicate schematically the occupation of bands as a function of strain.

Temperature-Dependent Photoluminescence. The temperature dependence of the luminescence of sample A, a pseudomorphic $Ge_{0.875}Sn_{0.125}$ alloy exhibiting a compressive strain of −1.65%, is shown in Figure 2a. A typical indirect-

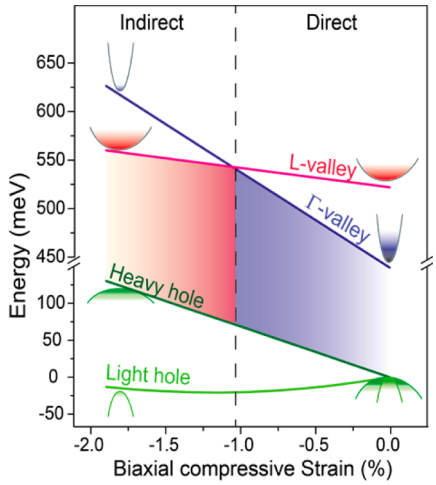

Figure 1. Calculated electronic band structure as a function of compressive strain for $Ge_{0.875}Sn_{0.125}$ alloys. The filled parabolas suggest the bands' occupation.

bandgap semiconductor behavior, known from Ge and dilute GeSn,[23] is observed: the room-temperature PL originating from electron−hole recombination at the center of the Brillouin zone (Γ-point) decreases in intensity with decreasing temperature and vanishes at about 100 K, due to the decreasing electron occupation of Γ-valley states, in the tail of the Fermi distribution. In the range of 100 K to 300 K, electrons located in the L-valley are thermally activated and are, thus, able to populate the Γ-valley. PL associated with indirect transitions is detected at 100 K and increases toward 4 K. The experimental activation energy of 47 meV is slightly below the theoretical energy difference between Γ- and L-valleys of 57 meV, indicating a fair agreement between calculations and experiment, considering the parameter uncertainties. Additionally, a second, weaker PL peak is detected at about 0.4 eV, labeled "D-lines". This is clearly resolved at low temperatures, and it does not shift with strain for the Sn content region discussed here. Its origin is not fully understood, yet; however, it may be related to defects at the Ge/GeSn interface.

The temperature-dependent PL changes substantially as the compressive strain in the GeSn layers drops below −1.05%. As an illustration, PL spectra of the direct-bandgap sample D at different temperatures are shown in Figure 2b. Here, the same scale but different multiplication factors are used to facilitate comparison. The PL intensity strongly increases at lower temperatures: the spontaneous emission intensity at 4 K is ~80 times higher than that at 295 K. The bandgap increases upon cooling; thus the Γ-valley luminescence is blue-shifted from 0.46 to 0.49 eV. The full width at half-maximum (fwhm) of the PL peak decreases from 52 meV at 295 K down to 24 meV at 4 K. The integrated PL intensity as a function of temperature of all investigated samples is displayed in Figure 2c. A methodology to discriminate a direct from an indirect fundamental bandgap using temperature-dependent PL measurements has been presented recently in ref 16. On the basis of the same arguments, samples B to E are fundamental direct-bandgap semiconductors, manifested by monotonically *increasing* PL with decreasing temperature, similarly to PL from direct-bandgap III−V alloys or dichalcogenides.[26,27] The fit of the integrated PL intensity using the joint density of state (JDOS) model (see refs 16 and 28 for model description and material parameters) offers for the strong direct-bandgap samples C−E

DOI: 10.1021/acsphotonics.5b00372
ACS Photonics 2015, 2, 1539−1545

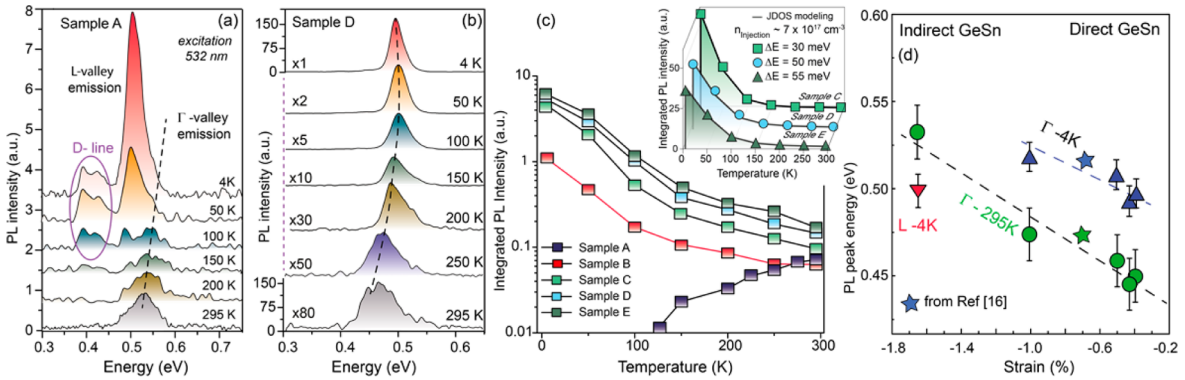

Figure 2. Temperature-dependent photoluminescence of (a) sample A, an indirect-bandgap GeSn alloy, and (b) sample D, a direct-bandgap GeSn alloy. (c) Evolution of the integrated PL of Γ-valley transitions for all samples. Inset: The fit of the integrated PL intensity for samples C–E using the JDOS model[16] gives a $\Delta E_{L\text{-}\Gamma}$ of 30, 50, and 55 meV, in good agreement with calculated values in Table 1, and an injected carrier density of about 7×10^{17} cm^{-3}. (d) Experimental extracted PL peak energies as a function of strain. The dotted lines serve as guide to the eye.

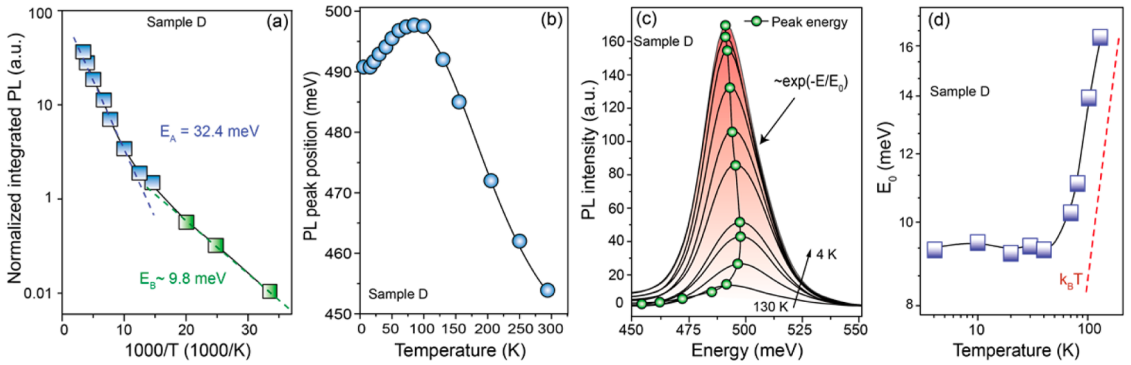

Figure 3. (a) Arrhenius plot of the normalized integrated PL used for the extraction of activation energies E_A and E_B at higher and lower temperatures, respectively. (b) Temperature dependence of PL peak energy and (c) PL spectra of sample D. (d) Extraction of specific energy E_0.

values for $\Delta E_{L\text{-}\Gamma}$ of 30, 50, and 55 meV, in good agreement with theoretical calculated values listed in Table 1 (inset of Figure 2c).

The luminescence enhancement with decreasing temperatures observed in low-directness samples B–E is predominantly attributed to the reduced transfer of electrons from Γ- into the L-valleys by thermal activation; thus, low temperatures result in a higher electron population of the Γ-valley. In general, the PL of direct-bandgap semiconductors decreases in intensity and the PL peak broadens with increasing temperature. This is ascribed to an exponential increase of nonradiative electron–hole recombination processes, including the fast diffusion of photocarriers toward surfaces and interfaces that leads to nonradiative surface and interface recombination, respectively, which reduces the radiative transition rate (with activation energy, E_A). The peak broadening is mainly due to the corresponding temperature-dependent broadening of the Fermi distribution of carriers within electronic bands. Based on ellipsometry measurements, the extinction coefficient of our samples is 2.2–2.3 at an excitation wavelength of 532 nm. This translates into an absorption coefficient $\alpha \approx 53\ \mu m^{-1}$. Consequently, the photocarriers are generated within an about 20 nm thin surface layer, and the surface recombination can, thus, be considered as nearly constant in all samples. However, the effect of nonradiative recombination at the GeSn/Ge-VS interface on the radiative recombination decreases for thicker layers; consequently, the PL intensity is enhanced. This effect is clearly observed by comparing samples with similar strain values but different thicknesses, e.g., in samples C–E (Figure 2c).

Notably, for the indirect sample A a stronger PL emission at 295 K is observed compared to the "just direct" ($\Delta E_{\Gamma\text{-}L} \approx 0$) sample B. This might be related to an increased nonradiative recombination due to the misfit dislocations at the GeSn/Ge-VS interface for the relaxed sample B. In indirect semiconductors with a low density of defects the photocarrier density can be substantially increased because of the long recombination time, which might be in the microsecond range.[29,30] Hence, despite the lower radiative recombination probability, the PL intensity for sample A might be higher than in sample B for the same illumination.

Furthermore, the theoretically predicted strain-dependent band structure (cf. Figure 1) and bandgap evolution[28] has been experimentally verified. The experimental linear strain dependence of the Γ-valley emission at 4 K and 295 K is shown in Figure 2d. The existence of a maximum in the bandgap evolution with compressive strain, however, can be shown only at low temperature. As a consequence, identical bandgaps for indirect- and direct-bandgap semiconductors can be observed in the same binary material system.[28] The L-valley emission (4 K) of sample A defining the bandgap of this alloy, at about 0.50 eV, is blue-shifted by only a few millielectronvolts compared to the direct transition in sample D.

Activation and Emission Energies. The activation energy, E_A, of nonradiative processes at higher temperature was obtained from the Arrhenius plot of the normalized integrated PL intensity[31] (Figure 3a) and is given in Table 1. As

DOI: 10.1021/acsphotonics.5b00372
ACS Photonics 2015, 2, 1539–1545

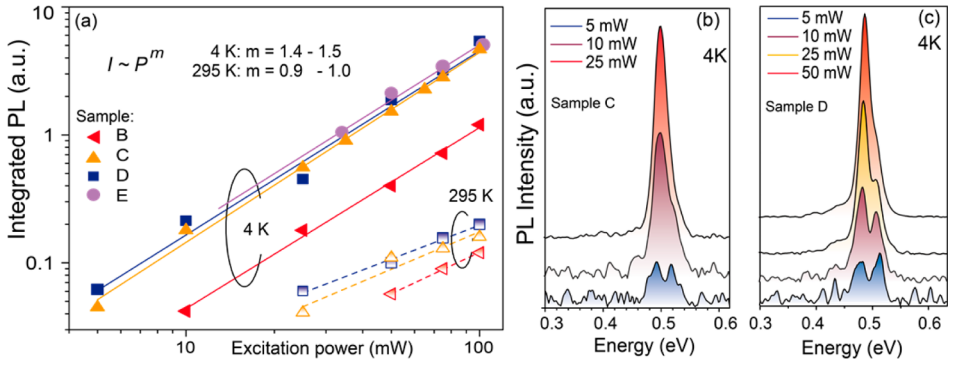

Figure 4. (a) Log–log plot of the excitation density versus integrated photoluminescence at different temperatures for different samples. (b, c) Power dependence of PL spectra of samples C and D showing the resolved Γ-LH and Γ-HH contributions. (Excitation wavelength 532 nm.)

expected, it increases with increasing directness $\Delta E_{\Gamma\text{-}L}$ and decreases for really thick layers (sample E) when degradation due to dislocation formation sets in. Besides the thermal activated photocarrier transfer between Γ- and L-valleys, which has a contribution to the temperature dependence of the PL, the usual decrease of the PL at high temperatures due to an increase of the nonradiative recombination affects the activation (deactivation) energy values. This may explain the differences between calculated $\Delta E_{L\text{-}\Gamma}$ and E_A in Table 1.

The temperature dependence of the peak energy provides information on the carrier distribution within electronic bands or localized states. Figure 3b depicts the temperature dependence (4–300 K) of the energy position of the PL peak for sample D. The corresponding PL spectra in the range 4–130 K are shown in Figure 3c. From 300 K down to 80 K the temperature dependence follows the bandgap (Varshni law[32]) and carrier distribution variation, but from 80 K to 4 K the PL peak steadily shifts to lower energies by approximately 7.5 meV. The circles in Figure 3c mark the peak energy positions up to 295 K. Their nonmonotonic temperature dependence may stem from electron localization in a fluctuating potential due to Sn content variations or bound excitons at trap centers, most likely Sn vacancies or other crystal defects. Its appearance at 80 K suggests a thermal energy of $k_B \cdot 80\ \text{K} \approx 7$ meV required to excite an electron from such a trap into the band and may be interpreted as the energy of a potential barrier. Similar PL temperature dependences have been observed in disordered, direct-gap III–V ternaries, such as InGaN[33] or InGaP,[34] but not in ordered binaries such as GaAs.

A more quantitative analysis can be made from the high-energy tail of the emission spectra using the Boltzmann approximation ($\sim\exp(E/E_0)$). Because of fast carrier thermalization in bands (~picoseconds)[35] and the high carrier energy compared to the intrinsic Fermi level, the high-energy tail of the PL spectra reflects the Boltzmann distribution of carriers. Here, E_0 correlates with the thermal energy k_BT. At $T < 80$ K, a constant value of $E_0 = 9$ meV is obtained (Figure 3d), which is in good agreement with the low-temperature activation energy E_B (Figure 3a) and the PL peak energy drop.

Pump Power Dependence. For most of the investigated samples, a pump power as low as 5 mW at 4 K is sufficient for PL signal detection, while at 295 K, the minimum laser power was increased to 25 mW (to minimize errors). The luminescence intensity, I, was fitted to $I \sim P^m$, where P is the optical excitation power. The exponent m is related to recombination mechanisms. For a low photocarrier density compared to the dark carrier density, an exponent $m \approx 1$ is expected. For a high carrier density the exponent $m \approx 1$ is expected if band-to-band recombination dominates, $m \approx 0.6$ for predominant Auger recombination, and $m \approx 2$ if nonradiative Shockley–Read–Hall recombination is the main process. The power dependence plotted in Figure 4a shows that the exponent changes from $m \approx 1.4$–1.5 at 4 K to about $m \approx 1$ at 295 K. A major assumption in this simplified picture is the spatial uniformity of the generation and recombination processes. In our case, where the pump absorption takes place in only a fraction of the layer thickness, a mixed regime is expected with intermediary values of the exponent. Additionally, the peculiarities of direct-bandgap recombination in the presence of HH-LH splitting and the decreasing Auger recombination lifetime with temperature[36] may explain the different m values.

The pump power dependence also allows resolving the contributions of Γ-HH and Γ-LH transitions. At $k = 0$ the Γ-HH transitions emit only in-plane polarized light (i.e., light perpendicular to the layer), while the Γ-LH transitions emit in any direction (3 times more in the in-plane than in the perpendicular direction). Experimentally, the PL is collected normal to the layer, so both transitions are observed. The emission peaks for both transitions are above rather than at the corresponding band edge energies. Under suitable conditions, low temperatures and low power densities as discussed below, the two peaks may be resolved within the full PL spectrum.

At 295 K the PL spectra show features ascribed to Fabry–Perot resonances due to the large Ge-VS thickness, which do not allow a clear separation between LH and HH contributions. However, at low temperatures the energy distribution of holes across the HH and LH bands at moderate hole concentrations of 10^{17}–10^{18} cm^{-3} allows sufficient HH and LH population to make both transitions clearly visible.[37] The PL spectra for samples C and D at 4 K and low pump power (Figure 4b,c) show two distinct contributions associated with Γ-HH and Γ-LH direct transitions. In intrinsic highly strained GeSn alloys, LH states should be filled with electrons (i.e., empty from holes) for low carrier densities; Γ-LH PL transitions should then be absent. However, the higher strain relaxation[11] reduces the HH–LH energy separation (Figure 1), resulting in an increased hole population of the LH band. This explains the coexistence of Γ-HH and Γ-LH transitions in the PL spectra of nearly fully relaxed layers at low pump powers. No Γ-band luminescence splitting appears for sample C at excitations above 25 mW but is observed in sample D up to 50 mW; then the emission is dominated by Γ-HH transitions at higher laser pumping power. To confirm that radiative recombination really

DOI: 10.1021/acsphotonics.5b00372
ACS Photonics 2015, 2, 1539–1545

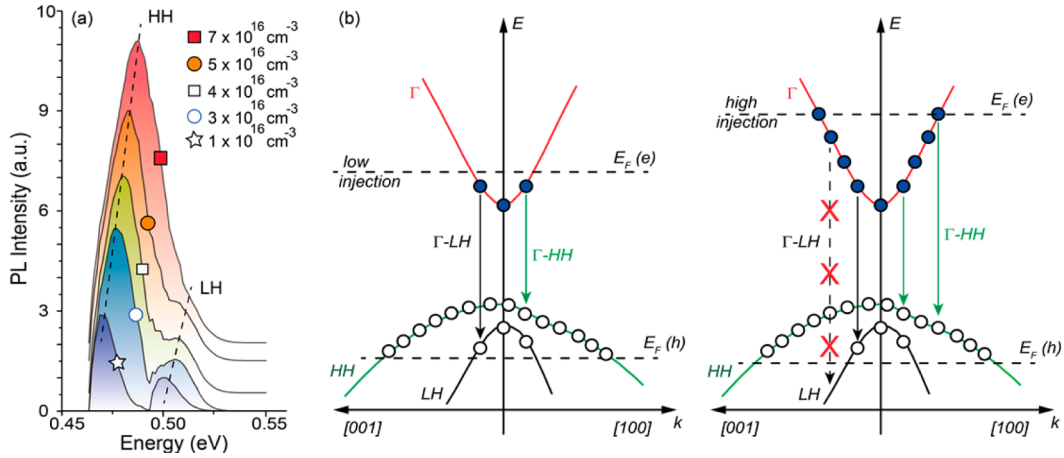

Figure 5. (a) Simulation of emission for different photocarrier generation levels. (b) Schematics of the Γ-LH and Γ-HH transitions under low and high optical excitations.

stems from recombination to both HH and LH bands and to understand the intensity dependence of the two transitions, emission spectra were simulated.

The PL spectra for a GeSn layer with a strain of −0.3% and a background hole density of 5×10^{18} cm^{-3} under optical pumping between 1×10^{16} and 7×10^{16} cm^{-3} are shown in Figure 5a. While the Γ-HH PL steadily increases with pumping, the Γ-LH emission saturates. In compressively strained layers the HH band is higher in energy and has a larger density of states than LH. Holes populate states from the top of HH or LH sub-bands down to the hole quasi-Fermi level, E_F(h) (see Figure 5b). When the electron density (excitation) increases, electrons first populate smaller k-wave vector states and recombine directly with holes from the HH and LH bands, with the same k-vectors. At larger electron density, an increased range of k-states in the Γ-valley becomes populated and only the HH band has holes with large k-vectors. Therefore, the Γ-HH emission increases. However, with no large-k LH states populated, the Γ-LH emission remains constant and is eventually swamped by the Γ-HH PL peak for sufficiently large pumping power. Such a behavior supports the conclusion about the direct character of the PL transitions. In the case of indirect transitions, such variations of k-vector are not important, because phonons are always involved in transitions. Furthermore, the conduction band filling, as the photocarrier density increases, leads to a blue shift of the PL peak with increasing pumping, a conventional feature of low-temperature PL.

CONCLUSIONS

In conclusion we have presented the first comprehensive study of the optical transitions in direct-bandgap $Ge_{0.875}Sn_{0.125}$ group IV alloys via PL measurements as a function of temperature and excitation power. The analysis of the integrated emission intensities allows clearly identifying a strain-dependent indirect- to direct-bandgap transition, in good agreement with our theoretical computations. Accordingly, pseudomorphic GeSn alloys on Ge-VS show a PL behavior specific to indirect-bandgap semiconductors, while layers with compressive strain of ≤1% were found to have a fundamental direct bandgap. The observed red shift of the PL at low temperatures might be attributed to alloy fluctuations. Low pumping power at low temperatures allows the observation of HH and LH splitting of the valence band. The calculated PL spectra dependence on photoexcitation level reproduces the PL shape evolution at low temperatures in direct-bandgap GeSn with small HH−LH splitting, which shows saturation of Γ-LH but no saturation of Γ-HH PL at high injection. These results provide additional evidence for the fundamental direct bandgap and the high crystalline quality of thick $Ge_{0.875}Sn_{0.125}$ layers grown on Ge virtual substrates. Direct-bandgap group IV alloys can thus be epitaxially grown on Ge/Si, offering simple but novel approaches for integrated photonics and electronics.

METHODS

Photoluminescence. The GeSn layers were investigated using a step-scan PL setup with lock-in technique. The samples were excited by a chopped frequency-doubled CW diode laser (532 nm wavelength) with a maximum power of 100 mW. The PL signal was collected into a Fourier transform infrared (FTIR) spectrometer and guided to a liquid-nitrogen-cooled InSb detector with a cutoff wavelength of 5.4 μm. The step-scan method has the advantage of eliminating the background thermal light from the spectrum. However, there is a transient signal at the beginning of the steps due to thermal radiation (even though the thermal radiation wavelength is outside the recorded range), which can perturb the measurements. The effect is stronger in the case of high amplification necessary for weak PL. To reduce this effect, a longer step waiting time is necessary and thus a longer acquisition time for a spectrum. In these cases, and for samples that clearly do not show emission at longer wavelengths, we eliminated the influence of thermal radiation by using a filter with a ∼3 μm cutoff placed in front of the detector.

Modeling. The PL spectrum has contributions from direct interband c.b.(Γ)−v.b.(Γ), direct intervalence band, and indirect (phonon-assisted) interband c.b.(L)−v.b.(Γ) transitions. These are all included, the last one according to the approximate model[38] because its contribution is small in this direct-gap system. The intervalence band contribution is also insignificant in the spectral range considered here and for hole densities expected in the system. The most important part is the direct interband luminescence and is calculated from the full 8 × 8 k·p model, which accounts for the warping and nonparabolicity of the valence and conduction bands. The direct luminescence rate (number of photons with polarization ε emitted per unit time per unit volume, per unit spectral interval) is calculated from

DOI: 10.1021/acsphotonics.5b00372
ACS Photonics 2015, 2, 1539−1545

$$R(\hbar\omega) = \frac{n_r \omega e^2}{3\pi c^3 \hbar \varepsilon_0 m_0^2} \frac{1}{(2\pi)^3} \sum_{\substack{\text{c.b.,v.b.} \\ \text{states}}} \int |\vec{\varepsilon} \cdot \overrightarrow{p_{cv}}(k)|^2 \times f_c(1 - f_v)\delta(E_c(k) - E_v(k) - \hbar\omega) d^3k$$

where $E_{v,c}(k)$ are the state energies in the valence and conduction band, p_{cv} is the transition matrix element, both dependent on the wave vector k and calculated with the states of the 8 × 8 $k{\cdot}p$ Hamiltonian with strain,[25] $f_c(E_c, E_{Fc}, T)$ and $f_v(E_v, E_{Fv}, T)$ are the electron distribution functions in the conduction and valence bands, respectively, with the Fermi levels $E_{Fc,v}$ determined from the carrier densities. All the parameters for the $k{\cdot}p$ calculation (Luttinger parameters, deformation potentials, bowing parameters for the alloy, etc.) and the refractive index n_r are listed in the Supporting Information of ref 16 with the source references given therein, ε_0 is the vacuum permittivity, and e and m_0 are the free electron charge and mass. Interband transitions are normally broad because of carrier distribution over nonequispaced states, and the integration was done by the linear tetrahedron method, rather than by replacing the δ-function by a Lorentzian.

AUTHOR INFORMATION

Corresponding Authors

*E-mail: d.gruetzmacher@fz-juelich.de.
*E-mail: d.m.buca@fz-juelich.de.

Author Contributions

⊥D. Stange and S. Wirths contributed equally to this work.

Notes

The authors declare no competing financial interest.

ACKNOWLEDGMENTS

This research received funding for CVD growth investigations from Federal Ministery of Education and Research (BMBF) under project UltraLowPow (16ES0060 K). The authors thank Richard Geiger and Dr. Hans Sigg, Paul Scherrer Institute, Switzerland, for making available their JDOS model.

REFERENCES

(1) Soref, R. A.; Perry, C. H. Predicted bandgap of the New Semiconductor SiGeSn. *J. Appl. Phys.* **1991**, *69*, 539.
(2) He, G.; Atwater, H. Interband Transitions in Sn X Ge 1-X Alloys. *Phys. Rev. Lett.* **1997**, *79*, 1937−1940.
(3) Moontragoon, P.; Ikonić, Z.; Harrison, P. Band Structure Calculations of Si−Ge−Sn Alloys: Achieving Direct bandgap Materials. *Semicond. Sci. Technol.* **2007**, *22*, 742−748.
(4) Eckhardt, C.; Hummer, K.; Kresse, G. Indirect-to-Direct Gap Transition in Strained and Unstrained SnxGe1−x Alloys. *Phys. Rev. B: Condens. Matter Mater. Phys.* **2014**, *89*, 165201.
(5) Attiaoui, A.; Moutanabbir, O. Indirect-to-Direct bandgap Transition in Relaxed and Strained Ge1−x−ySixSny Ternary Alloys. *J. Appl. Phys.* **2014**, *116*, 063712.
(6) Lu Low, K.; Yang, Y.; Han, G.; Fan, W.; Yeo, Y. Electronic Band Structure and Effective Mass Parameters of Ge1−xSnx Alloys. *J. Appl. Phys.* **2012**, *112*, 103715.
(7) Gupta, S.; Magyari-Köpe, B.; Nishi, Y.; Saraswat, K. C. Achieving Direct bandgap in Germanium through Integration of Sn Alloying and External Strain. *J. Appl. Phys.* **2013**, *113*, 073707.
(8) Fitzgerald, E. A.; Freeland, P. E.; Asom, M. T.; Lowe, W. P.; Macharrie, R. A.; Weir, B. E.; Kortan, A. R.; Thiel, F. A.; Xie, Y. H.; Sergent, A. M.; Cooper, S. L.; Thomas, G. A.; Kimerling, L. C. Epitaxially Stabilized GexSn1−x Diamond Cubic Alloys. *J. Electron. Mater.* **1991**, *20*, 489−501.
(9) Wirths, S.; Tiedemann, A. T.; Ikonic, Z.; Harrison, P.; Holländer, B.; Stoica, T.; Mussler, G.; Myronov, M.; Hartmann, J. M.; Grützmacher, D.; Buca, D.; Mantl, S. Band Engineering and Growth of Tensile Strained Ge/(Si)GeSn Heterostructures for Tunnel Field Effect Transistors. *Appl. Phys. Lett.* **2013**, *102*, 192103.
(10) Senaratne, C. L.; Gallagher, J. D.; Aoki, T.; Kouvetakis, J.; Menéndez, J. Advances in Light Emission from Group-IV Alloys via Lattice Engineering and N-Type Doping Based on Custom-Designed Chemistries. *Chem. Mater.* **2014**, *26*, 6033−6041.
(11) Von den Driesch, N.; Stange, D.; Wirths, S.; Mussler, G.; Holländer, B.; Ikonic, Z.; Hartmann, J. M.; Stoica, T.; Mantl, S.; Grützmacher, D.; Buca, D. Direct Bandgap Group IV Epitaxy on Si for Laser Applications. *Chem. Mater.* **2015**, *27*, 4693−4702.
(12) Ghetmiri, S. A.; Du, W.; Margetis, J.; Mosleh, A.; Cousar, L.; Conley, B. R.; Nazzal, A.; Sun, G.; Soref, R. A.; Tolle, J.; Li, B.; Naseem, H. A.; Ghetmiri, S. A.; Du, W.; Margetis, J.; Mosleh, A.; Cousar, L.; Tolle, J.; Li, B.; Naseem, H. A.; Yu, S. Direct-Bandgap GeSn Grown on Silicon with 2230nm Photoluminescence. *Appl. Phys. Lett.* **2014**, *105*, 151109.
(13) Vincent, B.; Gencarelli, F.; Bender, H.; Merckling, C.; Douhard, B.; Petersen, D. H.; Hansen, O.; Henrichsen, H. H.; Meersschaut, J.; Vandervorst, W.; Heyns, M.; Loo, R.; Caymax, M. Undoped and in-Situ B Doped GeSn Epitaxial Growth on Ge by Atmospheric Pressure-Chemical Vapor Deposition. *Appl. Phys. Lett.* **2011**, *99*, 152103.
(14) Xie, J.; Chizmeshya, A. V. G.; Tolle, J.; D'Costa, V. R.; Menendez, J.; Kouvetakis, J. Synthesis, Stability Range, and Fundamental Properties of Si−Ge−Sn Semiconductors Grown Directly on Si(100) and Ge(100) Platforms. *Chem. Mater.* **2010**, *22*, 3779−3789.
(15) Wirths, S.; Ikonic, Z.; Tiedemann, A. T.; Holländer, B.; Stoica, T.; Mussler, G.; Breuer, U.; Hartmann, J. M.; Benedetti, A.; Chiussi, S.; Grützmacher, D.; Mantl, S.; Buca, D. Tensely Strained GeSn Alloys as Optical Gain Media. *Appl. Phys. Lett.* **2013**, *103*, 192110.
(16) Wirths, S.; Geiger, R.; von den Driesch, N.; Mussler, G.; Stoica, T.; Mantl, S.; Ikonic, Z.; Luysberg, M.; Chiussi, S.; Hartmann, J. M.; Sigg, H.; Faist, J.; Buca, D.; Grützmacher, D. Lasing in Direct-Bandgap GeSn Alloy Grown on Si. *Nat. Photonics* **2015**, *9*, 88−92.
(17) Ackert, J. J.; Thomson, D. J.; Shen, L.; Peacock, A. C.; Jessop, P. E.; Reed, G. T.; Mashanovich, G. Z.; Knights, A. P. High-Speed Detection at Two Micrometres with Monolithic Silicon Photodiodes. *Nat. Photonics* **2015**, *9*, 393−396.
(18) Zhang, H.; Kavanagh, N.; Li, Z.; Zhao, J.; Ye, N.; Chen, Y.; Wheeler, N. V.; Wooler, J. P.; Hayes, J. R.; Sandoghchi, S. R.; Poletti, F.; Petrovich, M. N.; Alam, S. U.; Phelan, R.; O'Carroll, J.; Kelly, B.; Grüner-Nielsen, L.; Richardson, D. J.; Corbett, B.; Garcia Gunning, F. C. 100 Gbit/s WDM Transmission at 2 Mm: Transmission Studies in Both Low-Loss Hollow Core Photonic Bandgap Fiber and Solid Core Fiber. *Opt. Express* **2015**, *23*, 4946.
(19) Soref, R. Group IV Photonics: Enabling 2 Mm Communications. *Nat. Photonics* **2015**, *9*, 358−359.
(20) Homewood, K. P.; Lourenço, M. a. Optoelectronics: The Rise of the GeSn Laser. *Nat. Photonics* **2015**, *9*, 78−79.
(21) Chen, R.; Lin, H.; Huo, Y.; Hitzman, C.; Kamins, T. I.; Harris, J. S. Increased Photoluminescence of Strain-Reduced, High-Sn Composition Ge1−xSnx Alloys Grown by Molecular Beam Epitaxy. *Appl. Phys. Lett.* **2011**, *99*, 181125.
(22) Du, W.; Ghetmiri, S. A.; Conley, B. R.; Mosleh, A.; Nazzal, A.; Soref, R. A.; Sun, G.; Tolle, J.; Margetis, J.; Naseem, H. A.; Yu, S.-Q. Competition of Optical Transitions between Direct and Indirect Bandgaps in Ge1−xSnx. *Appl. Phys. Lett.* **2014**, *105*, 051104.
(23) Ryu, M.-Y.; Harris, T. R.; Yeo, Y. K.; Beeler, R. T.; Kouvetakis, J. Temperature-Dependent Photoluminescence of Ge/Si and Ge1-ySny/Si, Indicating Possible Indirect-to-Direct Bandgap Transition at Lower Sn Content. *Appl. Phys. Lett.* **2013**, *102*, 171908.
(24) Hartmann, J. M.; Abbadie, A.; Cherkashin, N.; Grampeix, H.; Clavelier, L. Epitaxial Growth of Ge Thick Layers on Nominal and 6° off Si(0 0 1); Ge Surface Passivation by Si. *Semicond. Sci. Technol.* **2009**, *24*, 055002.

DOI: 10.1021/acsphotonics.5b00372
ACS Photonics 2015, 2, 1539−1545

(25) Bahder, T. Eight-Band K·p Model of Strained Zinc-Blende Crystals. *Phys. Rev. B: Condens. Matter Mater. Phys.* **1990**, *41*, 11992−12001.
(26) Lezama, I. G.; Arora, A.; Ubaldini, A.; Barreteau, C.; Giannini, E.; Potemski, M.; Morpurgo, A. F. Indirect-to-Direct bandgap Crossover in Few-Layer MoTe2. *Nano Lett.* **2015**, *15*, 2336−2342.
(27) Peng, X.; Wei, Q.; Copple, A. Strain-Engineered Direct-Indirect bandgap Transition and Its Mechanism in Two-Dimensional Phosphorene. *Phys. Rev. B: Condens. Matter Mater. Phys.* **2014**, *90*, 1−10.
(28) Schulte-Braucks, C.; Stange, D.; von den Driesch, N.; Blaeser, S.; Ikonic, Z.; Hartmann, J. M.; Mantl, S.; Buca, D. Negative Differential Resistance in Direct Bandgap GeSn P-I-N Structures. *Appl. Phys. Lett.* **2015**, *107*, 042101.
(29) Stoica, T.; Vescan, L. Quantum Efficiency of SiGe LEDs. *Semicond. Sci. Technol.* **2003**, *18*, 409−416.
(30) Gaubas, E.; Vanhellemont, J. Comparative Study of Carrier Lifetime Dependence on Dopant Concentration in Silicon and Germanium. *J. Electrochem. Soc.* **2007**, *154*, H231.
(31) Chtchekine, D.; Feng, Z.; Chua, S.; Gilliland, G. Temperature-Varied Photoluminescence and Magnetospectroscopy Study of near-Band-Edge Emissions in GaN. *Phys. Rev. B: Condens. Matter Mater. Phys.* **2001**, *63*, 1−7.
(32) Varshni, Y. P. Temperature Dependence of the Energy Gap in Semiconductors. *Physica* **1967**, *34*, 149−154.
(33) Teo, K. L.; Colton, J. S.; Yu, P. Y.; Weber, E. R.; Li, M. F.; Liu, W.; Uchida, K.; Tokunaga, H.; Akutsu, N.; Matsumoto, K. An Analysis of Temperature Dependent Photoluminescence Line Shapes in InGaN. *Appl. Phys. Lett.* **1998**, *73*, 1697.
(34) Driessen, F. A. J. M.; Bauhuis, G. J.; Olsthoorn, S. M.; Giling, L. J. Effects of Confined Donor States on the Optical and Transport Properties of Ordered GaInP2 Alloys. *Phys. Rev. B: Condens. Matter Mater. Phys.* **1993**, *48*, 7889−7896.
(35) Ohnishi, H.; Tomita, N.; Nasu, K. Real Time Relaxation Dynamics of Macroscopically Photo-Excited Electrons toward the Fermi Degeneracy Formation in the Conduction Band of Seniconductors. *J. Phys. Soc. Jpn.* **2015**, *84*, 1−4.
(36) Sun, G.; Soref, R. a.; Cheng, H. H. Design of an Electrically Pumped SiGeSn/GeSn/SiGeSn Double-Heterostructure Midinfrared Laser. *J. Appl. Phys.* **2010**, *108*, 033107.
(37) Harris, T. R.; Yeo, Y. K.; Ryu, M.; Beeler, R. T.; Kouvetakis, J. Observation of Heavy- and Light-Hole Split Direct Bandgap Photoluminescence from Tensile-Strained GeSn (0.03% Sn). *J. Appl. Phys.* **2014**, *116*, 103502.
(38) Virgilio, M.; Manganelli, C. L.; Grosso, G.; Pizzi, G.; Capellini, G. Radiative Recombination and Optical Gain Spectra in Biaxially Strained N-Type Germanium. *Phys. Rev. B: Condens. Matter Mater. Phys.* **2013**, *87*, 235313.

DOI: 10.1021/acsphotonics.5b00372
ACS Photonics 2015, 2, 1539−1545